Nuclear Instruments and Methods in Physics Research B 553 (2024) 165398

Contents lists available at ScienceDirect

Nuclear Inst. and Methods in Physics Research, B

journal homepage: www.elsevier.com/locate/nimb

Full Length Article

Correlation of optical transmittance and hydrogen concentration in Cr/V superlattices

Theofanis Tsakiris [a,*], Kristina Komander [a], Max Wolff [a], Robert J.W. Frost [a], Sotirios A. Droulias [a], Gunnar K. Pálsson [a], Daniel Primetzhofer [a,b]

[a] Department of Physics and Astronomy, Uppsala University, S-751 20, Box 516, Uppsala, Sweden
[b] Tandem Laboratory, S-751 21, Box 529, Uppsala, Sweden

A B S T R A C T

We assess the linearity between the reduction of the optical transmittance in the wavelength range of 600–1000 nm and the hydrogen concentration in Cr/V hydrogenated superlattice structures, with a nominal Cr/V ratio of 2/14. The V layers, contained inside an epitaxial Cr/V superlattice, were exposed to gaseous H atmosphere. The hydrogen uptake, as well as the changes in their optical properties, due to the hydrogenation, were monitored through optical transmittance measurements. The resonant $^{1}H(^{15}N,\alpha\gamma)^{12}C$ nuclear reaction was used to obtain the hydrogen depth profile and to determine the average hydrogen concentration per host atom in the V layers. Linearity was experimentally confirmed between the change in optical transmittance in a wide wavelength range and the H concentration, showing that optical data can be used to extract the relative hydrogen concentration. Additionally, the changes in the optical transmittance of the superlattice were found to be more pronounced for incident light with a wavelength of 600 nm, while the corresponding optical changes in the wavelength range 700–1000 nm, presented negligible dependence on the wavelength.

1. Introduction

Transition metals can absorb hydrogen reversibly in large quantities, making them interesting to be used as hydrogen storage materials, in a hydrogen economy [1]. Hydrogen storage in these materials allows higher H volumetric density and improved safety, compared to high-pressure gas containers [2,3]. Interstitial vanadium hydrides are of particular interest since they exhibit higher gravimetric storage capacity [4] than hydride systems based on heavier transition metals, favorable kinetics [5] at ambient conditions, as well as a low heat of formation. This low heat of formation allows release of hydrogen at temperatures below 300 °C. However, hydrogenation/dehydrogenation cycles at a temperature below the critical temperature can cause mechanical strain, originating from the co-existence of different phases, pulverizing the material. In bulk vanadium, the solid-solution α-phase is disordered with hydrogen occupying tetrahedral T sites, while the β-phase is characterized by occupation of O sites, with the β_1 phase being ordered and the β_2 phase being disordered. In order to suppress the phase co-existence and preserve the integrity of the storage material, the loading of hydrogen needs to take place in a temperature that surpasses the critical temperature. Nanostructured systems, featuring a high surface-to-volume ratio, can exhibit thermodynamic properties that are even more favorable for applications, compared to their bulk counterparts, due to improved reaction kinetics [6] and reduced critical temperature [7] of the phase transition between α and β-phase. Furthermore, the effect of finite size [7], strain [8,9] and proximity of other, non-absorbing layers on the thermodynamics of hydrogenation of vanadium have been addressed with model systems such as Fe/V and Cr/V superlattices and shed light on the underpinning mechanisms, yet the question of the hydrogen occupancy has not been fully resolved.

The preferred occupancy has been extensively studied for different phases in bulk systems [10] and it has been found to be sensitive to the presence of strain [8,9,11,12,13]. The interstitial hydrogen atoms interact with each other through long-range elastic forces [14], that are mediated by the host metal. To gain insight into the effects of finite size [7], proximity and stress on hydrogen absorption, superlattice structures have been used as model systems [15]. Superlattice structures can be grown epitaxially [16,17,18] with precise control of the layer thickness, allowing for investigations in systems of different sizes and under different strain conditions. Diffusion [19], EXAFS [20] and XRD [13,21] studies have indicated octahedral occupation in Fe/V superlattices, which is supported by recent real-space channeling studies [22,23] where hydrogen was confirmed to occupy octahedral sites in Fe/V superlattice structures for high H/V concentrations.

Certain metal hydride systems have been found to change their optical properties by undergoing metal-to-semiconductor phase transitions

* Corresponding author.
E-mail address: theofanis.tsakiris@physics.uu.se (T. Tsakiris).

https://doi.org/10.1016/j.nimb.2024.165398
Received 30 January 2024; Received in revised form 2 May 2024; Accepted 11 May 2024
Available online 29 May 2024

[24]. However, even without a change in the phase, information on the thermodynamic properties of metal hydrides can be extracted by monitoring the changes in the optical transmittance for thin films on transparent substrates [25,26]. Such effects are currently being exploited in the context of hydrogen sensors [27,28]. Recently [29], a linear relation between the change of optical transmittance of red light upon deuterium absorption was confirmed for Fe/V and Cr/V 2/14 superlattices by combined optical transmission and neutron reflectometry measurements. Linearity was also verified in Fe/V hydrogenated superlattices, using nuclear reaction analysis (NRA) [30]. At present, the Cr/V system has not been studied as extensively as the Fe/V system, even though a very distinct behavior of the two aforementioned systems in excess resistivity upon hydrogenation [31] and hydrogen uptake [32] has been revealed. In this study, we assessed the linearity of the optical transmittance reduction, in the visible light spectrum, with respect to hydrogen concentration, in Cr/V superlattices, using NRA and optical transmittance measurements. The results of this study offer the means to convert changes in optical transmittance to hydrogen concentration for the Cr/V system, for a wide wavelength range, namely 600–1000 nm. Additionally, the presence of a compact dataset, in a wide wavelength range, will allow the comparison of the Cr/V system with more extensively studied systems, such as Fe/V.

In vanadium, the presence of interstitial hydrogen triggers a hybridization between the 1s orbital of H and the 3d band of V, inducing changes in the density of states, with the most profound changes being observed approximately 7 eV below the Fermi energy [33]. Similar changes in the electronic structure have been observed in Fe/V superlattices [34]. Additionally, the absorption of interstitial hydrogen induces a volume expansion $\frac{\Delta V}{V}$, which is linearly dependent on the hydrogen concentration c, through an expansion coefficient k $\left(\frac{\Delta V}{V} = kc\right)$, for a given hydrogen site occupancy [35]. For the case of epitaxial structures, the registry with the substrate induces uniaxial strain. Recent DFT calculations predict changes to the electric dipole tensor, and thus the transmittance, due to uniaxial expansion of the vanadium unit cell [29]. Hydrogen-induced changes to the optical properties, i.e. the transmitted intensity I, can be quantified by the Beer-Lambert law: $I = I_0 e^{-ad}$, which expresses an exponential reduction of the incident intensity I_0, based on a wavelength-dependent absorption coefficient *a*. Both *a* and *d* are expected to change due to the hydrogenation. Experimental determination of the changes in thickness *d*, combined with the change in optical intensity *I*, could give information on the absorption coefficient, and therefore the band structure. An average of the changes in optical transmittance upon hydrogenation can be assessed by comparing the transmitted intensity $-\ln\left(\frac{I(c)}{I(c=0)}\right)$ for a non-hydrogenated and a hydrogenated sample.

2. Methods

2.1. Sample preparation

Fig. 1 illustrates the Cr/V superlattice structure utilized in this work. The full details of the growth process, as well as detailed diffraction and reflectometry analysis of both the Fe/V and Cr/V systems, are described in [36]. Alternating V and Cr layers were grown epitaxially by DC magnetron sputtering on a MgO (0 0 1) single crystalline substrate, with a nominal Cr/V ratio of 2/14 monolayers (ML), repeated 23 times, with an additional 14 ML of V on top. The registry of the V, lattice constant a = 3.024 Å [37], and Cr layers to the MgO substrate, with an interatomic distance of d = 2.98 Å in the 110 plane, requires the ⟨1 0 0⟩ crystalline direction of the grown V to be parallel with the ⟨1 1 0⟩ crystalline direction of the MgO. During the epitaxial growth the roughness of the interatomic layers is not expected to exceed 1 ML, as seen in the study of the sibling Fe/V system, grown under identical conditions [17]. The

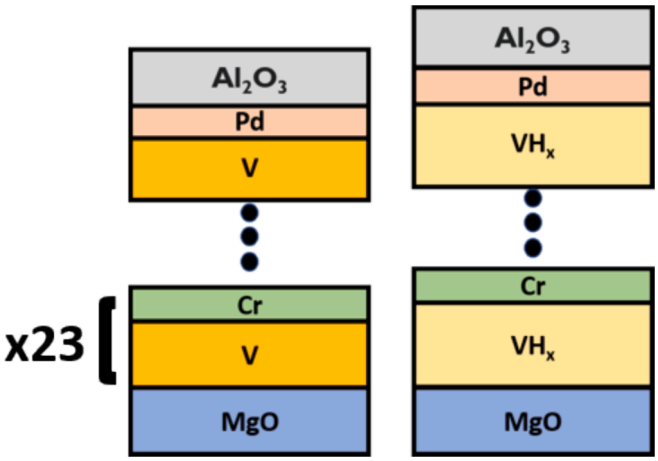

Fig. 1. Schematic representation of the Cr/V superlattice structure prior to (left part) and after (right part) absorbing hydrogen. The formation of the hydride phase leads to out-of-plane expansion.

lattice mismatch results in compressive in-plane stress on V, causing out-of-plane expansion of approximately 1.5 % [36]. The V layers in the superlattice therefore exhibit locally a base centered tetragonal-like symmetry. Due to the clamping with the substrate, volume expansion occurs primarily along the out-of-plane direction [20]. A thin Pd layer of 7 nm was grown for oxidization protection and for facilitating the dissociation of H_2 molecules. Due to the differences in the lattice constants of Pd and V [37], the former does not grow epitaxially. A capping of amorphous aluminum oxide was added using reactive magnetron sputtering. This oxide layer acts as a diffusion barrier [38] to allow the NRA measurements, which were performed in vacuum. The thickness of the aluminum oxide layer was later estimated from the NRA data to be approximately 22.5 nm, but an exact value was not obtained, as it does not directly affect any of the results of this study.

2.2. Hydrogen loading and optical measurements

Hydrogen loading was investigated by measuring the optical transmittance, in the wavelength range of 200–1000 nm using a self-stabilized polychromatic light source, while applying a defined hydrogen gas pressure, in a dedicated setup [39]. The steps of the hydrogen loading procedure are presented in Fig. 2. The optical transmittance measurement was averaged over the wavelength range of 630–1000 nm. As presented in Fig. 2, the duration of an average loading experiment is in the order of 20 h. The background signal from the room lighting was negligible compared to the intensity of the focused light source, as verified by optical spectra acquired with the light source turned off.

Prior to each loading process, the sample was annealed at 140 °C for several hours at ultra-high vacuum (UHV) conditions to remove any remaining hydrogen from the vanadium layers. The sample was then cooled to room temperature to obtain a reference value for the transmission spectrum of the non-hydrogenated state. Afterwards, the sample was reheated to 140 °C and exposed to gaseous hydrogen, of 99.999 mol % purity, of pressures in the range of 0.05–200 mbar. The observed decrease of the transmittance during the heating stage and prior to the introduction of the H_2 gas, could potentially be attributed to a temperature dependence of the refractive index of the V layers. The aforementioned transmittance reduction was not observed during the heating of a pristine MgO substrate, therefore it does not originate from it. Hydrogenation occurs exothermically only in the V layer (ΔH_{bulk} = -0.3 eV/atom) [40], while MgO and Cr [41] do not absorb hydrogen, in the temperature range used in this study. Palladium is not expected to absorb more than 4 % hydrogen for the temperature and pressure range

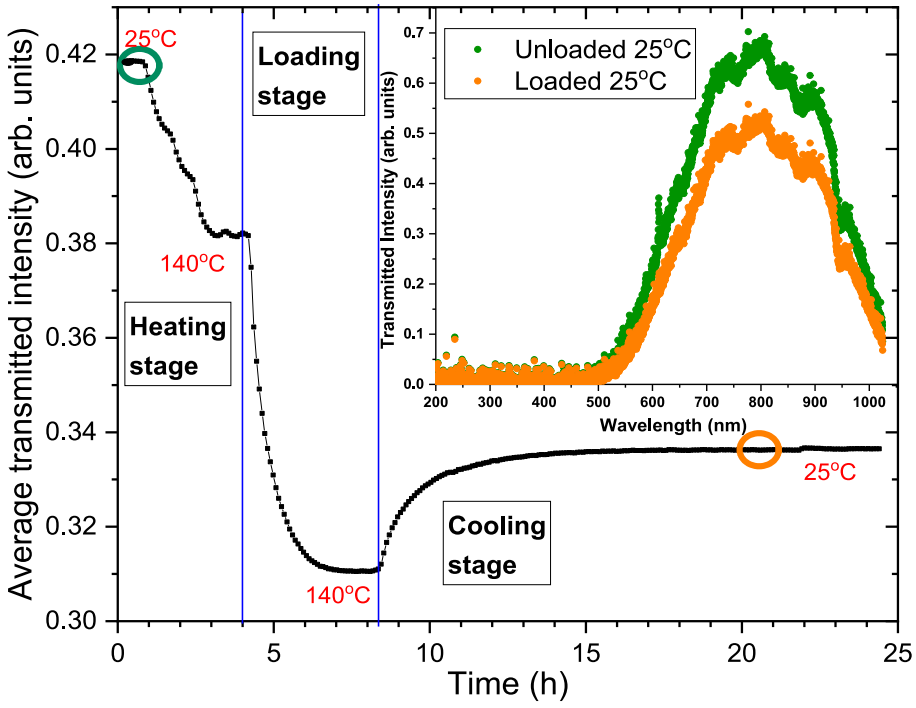

Fig. 2. Time evolution of the statistical average of the optical transmittance in the wavelength range of 630–1000 nm, in a typical loading experiment (H_2 loading pressure: 2 mbar). Inset: Optical transmittance spectra recorded at room temperature prior to (green) and after (orange) the hydrogenation process. (For interpretation of the references to colour in this figure legend, the reader is referred to the web version of this article.)

[42] investigated in this work. For such low H/Pd concentrations, the dielectric function of Pd, in the wavelength range studied, presents negligible changes [43]. The presence of aluminum oxide capping slowed down the absorption of the hydrogen, but is not expected to affect the optical properties in any way. The contribution of blackbody radiation from the heated sample to the measured optical spectrum was verified to be negligible, as the optical transmittance background spectra with the sample at room temperature and heated up to 140 °C were similar. In order to verify that the optical properties of the non-hydrogenated sample recover to their original value upon return to room temperature, the sample was repetitively annealed at 140 °C and cooled down, in a separate measurement, while monitoring its optical transmittance.

The stability of the optical transmittance over time indicated that equilibrium had been reached in each stage of the experiment and simultaneously confirmed the absence of any significant intensity drifts over the course of a few hours. Optical spectra corresponding to the non-hydrogenated and the hydrogenated state, at room temperature are illustrated in the inset of Fig. 2, showing the reduction of the optical transmittance, for all wavelengths in the range of 600–1000 nm.

Finally, the H_2 gas was pumped out of the chamber, while the sample was simultaneously cooling down. When the sample temperature had reached 60–70 °C, the pressure of the chamber was already in the UHV regime. During this simultaneous cooling and the pumping out of the H_2 gas, the aluminum oxide capping reduces hydrogen desorption at elevated temperature sufficiently to retain the hydrogen until the sample is cooled to room temperature. The hydrogen in the sample remains stable for the duration of the subsequent ion beam analysis experiment. Using this method of following a high temperature isotherm and quenching at room temperature, a wide range of hydrogen concentrations can be achieved.

2.3. Ion beam analysis

Ion beam analysis for quantitative hydrogen depth profiling was performed using the 5MV 15SDH-2 pelletron tandem accelerator [44], at the Tandem laboratory at Uppsala University. The absolute hydrogen concentration in the Cr/V layers of the superlattice was extracted through the use of the 6.385 MeV resonance of the $^{1}H(^{15}N,\alpha\gamma)^{12}C$ nuclear reaction. The nominal width of this resonance is equal to 1.8 keV. During the irradiation, the ^{15}N primary ion-beam current was kept below 1.5 nA and the beam spot was broadened to an approximate area of 20 mm^2 in order to avoid beam-induced hydrogen losses [45]. The 4.43 MeV gamma rays, originating from the deexcitation of $^{12}C^*$, were detected using a bismuth germanate (BGO) scintillation detector placed behind the sample. A lead shield was used to reduce the gamma background radiation from the naturally occurring radioactive nuclides [30], leading to lower dead time in the detector and less pile-up events in the gamma spectrum. In the energy range of interest, the signal from cosmic ray muons is virtually the sole background contribution. Gamma background spectra were acquired prior to each NRA measurement in order to perform the background subtraction.

Starting from an energy of 6.37 MeV, the beam energy of the ^{15}N primary ions was increased in steps of 15 keV, up to a maximum value of 6.7 MeV, positioning the resonance at different depths of the sample. The off-resonance contributions were considered negligible since the resonance cross section is 4 orders of magnitude larger than the corresponding off-resonance cross section [46]. The energy resolution of the experiment is governed by the doppler broadening originating from the zero-point vibration of hydrogen [47], which corresponds to a FWHM contribution of approximately 12 keV, the energy distribution of the primary beam, as well as the energy straggling of the ion beam in the material, which is dependent on the depth. The energy scans were repeated in backwards direction to verify the absence of hydrogen loss during the irradiation. The acquisition time for a spectrum was varied between 200 and 250 sec, leading to a statistical error, per point, from 7 % and up to 30 % for the high and low concentrations, respectively.

The absolute hydrogen concentration was obtained in a relative measurement, which eliminates the need for precise knowledge of the cross section and the solid angle of the detector [48]. The reference sample used in the present study was a standard of H-implanted silicon, with a nominal concentration of $C_H = 18.5$ %. The following formula

was applied to calculate the hydrogen concentration:

$$n_H = \frac{Y_{Cr/V}}{Y_{ref}} \frac{N_{ref}}{N_{Cr/V}} \frac{S_{Cr/V}}{S_{ref}} n_{ref} \quad (1)$$

In Eq. (1), Y denotes the gamma-ray yield, n the atomic density of H, N the total number of incoming ions and S the stopping power, of the reference sample and the Cr/V superlattice. The scattering chamber was electrically isolated, which allowed for the integration of the current of the primary beam, in order to determine the $N_{ref}/N_{Cr/V}$ ratio. The stopping power for the hydrogenated Cr/V was calculated using an iterative approach. First the sample was assumed to be pure Cr/V and an initial hydrogen concentration was obtained using formula (1). The SRIM [49] software package was used to obtain the initial stopping power values for the Cr/V layer. The stopping power values produced by the SRIM software for ^{15}N primary ions on V have recently been found to agree within 2 % with experimental values, with the contribution of hydrogen to the compound stopping being modelled according to SRIM to 64.55 eV/10^{15} $\frac{at}{cm^2}$, as experimentally verified for a range of high H concentrations [50]. Using the hydrogen concentration calculated from the previous step, a hydrogenated compound was then modeled and a new stopping power was extracted. This new stopping power led, through (1), to a new hydrogen concentration. After completing 3–4 steps of this iterative procedure of calculating the stopping power and the hydrogen concentration, the difference in the hydrogen concentration between subsequent iterations was below 0.1 % and considered as converged. The hydrogen concentration was converted to a H/V atomic ratio, using the atomic density of the clamped V, corrected for the atomic fraction of Cr, which had been verified through in-house RBS measurements, using 2 MeV ^{4}He ions, prior to this study. It should be noted that RBS did not feature sufficient depth resolution to resolve the signals from the Cr and V layers.

3. Results and discussion

3.1. NRA results

Fig. 3 illustrates the hydrogen concentration, in number of hydrogen atoms per vanadium, versus the energy of the probing ^{15}N beam. A surface peak is observed at 6.4 MeV and corresponds to hydrogen accumulated in surface contaminants and in the first layers of the aluminum oxide capping. The Pd layer could not be resolved with the energy resolution available, but since it is expected to absorb negligible hydrogen it is contributing in the intensity dip at 6.46 MeV. The energy difference of 60 keV between the surface peak and the Pd dip, in the NRA spectrum, hints a thickness of approximately 22.5 nm for the surface Al_2O_3 layer, assuming a stopping power of 2.67 eV/nm, obtained from SRIM software. The V layers absorb hydrogen, while the Cr layers do not, however the energy resolution of the present measurement was not sufficient to resolve these layers. As a result, an intensity plateau was present in the obtained gamma excitation function. For each loading experiment the hydrogen concentration was obtained based on the average gamma yield in the 6.505–6.64 MeV range, excluding the interface regions with the Pd layer and the MgO substrate. The averaging range was kept the same in the analysis of all measurements. For pressures lower than 0.25 mbar the hydrogen concentration is observed to be increased in the energy range 6.60–6.65 MeV, which corresponds to approximately the first 15 nm close to the MgO interface. This near-interface enhancement of the hydrogen signal has been observed in the literature for Fe/V superlattices with low H/V concentrations [30] and could potentially be attributed to hydrogen occupying defect states near the V/MgO interface, resulting from the difference in lattice parameters between MgO and V.

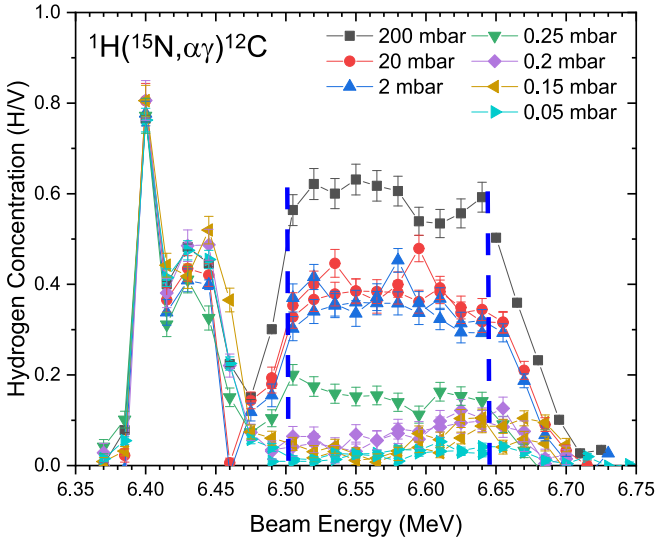

Fig. 3. Hydrogen concentration versus the energy of the ^{15}N primary beam, for the Cr/V superlattice, for different nominal loading pressures. The dashed blue lines highlight the energy region of 6.505–6.64 MeV, that was used to obtain the average gamma yield, for each loading. (For interpretation of the references to colour in this figure legend, the reader is referred to the web version of this article.)

3.2. Optical transmission spectroscopy – wavelength dependence of the hydrogen induced changes

The ratio of the transmitted intensity of the hydrogenated state, at different concentrations, versus the intensity from the non-hydrogenated state, is presented in Fig. 4, for the wavelength range of 550–1000 nm. This ratio is obtained though the following procedure: Several post-hydrogenation transmittance spectra, at room temperature, are averaged into one spectrum, which will be referred to as the hydrogenated spectrum. In the same manner, room temperature spectra, prior to the hydrogenation, are averaged into one spectrum, which will be referred to as the non-hydrogenated spectrum. The number of spectra that were used to obtain the average spectrum in both of these cases can vary in number from 5 to 50, but they were always chosen from a time window of apparent optical stability. The hydrogenated spectrum is then divided (point by point) by the non-hydrogenated spectrum in order to obtain the ratio depicted in Fig. 4. The intensity of the light source in the wavelength region <550 nm was low, resulting in a higher noise-to-signal ratio in this regime for all loading experiments and is therefore omitted. The spectral lines around 620 nm have been identified as scattered light from the laboratory ceiling lighting, and are excluded in the analysis. The hydrogenated superlattice exhibits up to 35 % lower transmittance compared to the unloaded system. As the H_2 pressure increases, a higher hydrogen concentration is achieved, up to approximately 0.6 H/V in this experiment. The results are consistent with high-temperature isotherm data that are available in the literature [25] for thin VH_x layers. As demonstrated in the next section, the ratios presented in Fig. 4 were not found constant over the 600–1000 nm wavelength range studied, with the wavelength dependence of the reduction of the optical transmittance of the Cr/V superlattice, being more pronounced at lower wavelengths.

3.3. Correlation of optical and NRA results

To further assess the wavelength-dependent changes in the spectrum, five optical regions of interest, namely 600 ± 5, 700 ± 5, 800 ± 5, 900 ± 5 and 1000 ± 5 nm, were chosen to study the response to hydrogenation. In each region of interest, the average transmitted intensity ratio, denoted as I(c)/I(0), was extracted. Fig. 5 presents the optical changes, expressed in negative logarithm of the intensity ratio, versus the hydrogen concentration, in units of hydrogen per host V atom. The

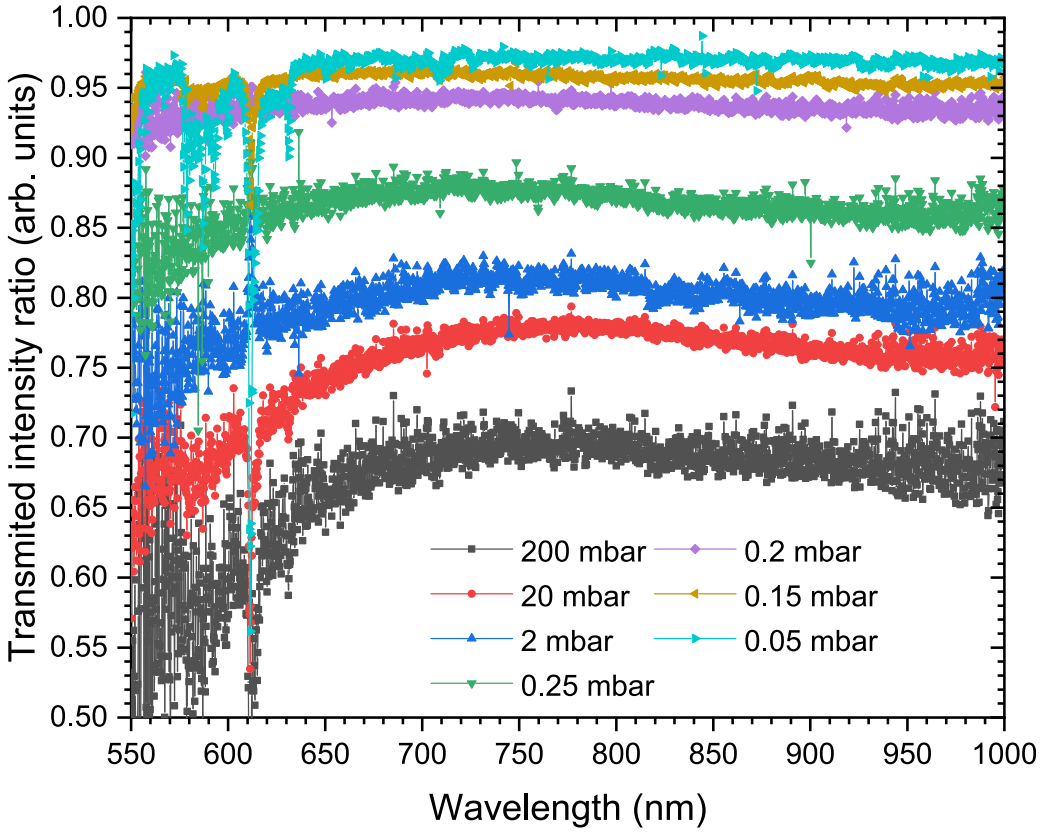

Fig. 4. Ratio of the transmitted intensity through the hydrogenated sample versus the transmitted intensity through the non–hydrogenated sample, at room temperature, in the wavelength range of 550–1000 nm, for different nominal loading pressures.

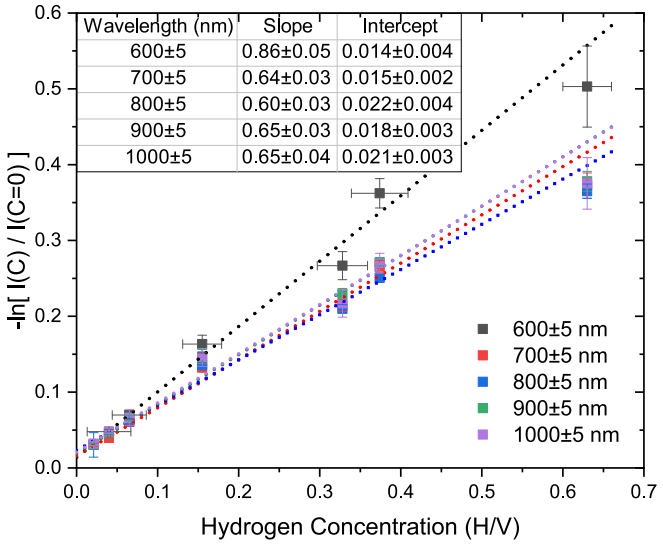

Wavelength (nm)	Slope	Intercept
600±5	0.86±0.05	0.014±0.004
700±5	0.64±0.03	0.015±0.002
800±5	0.60±0.03	0.022±0.004
900±5	0.65±0.03	0.018±0.003
1000±5	0.65±0.04	0.021±0.003

Fig. 5. Changes in optical transmittance, at room temperature, versus the hydrogen concentration, in H per V atom, for different wavelengths of incident light in the range of 600–1000 nm. The dotted lines represent the curves obtained from linear fitting. Inset table: Slopes and intercepts extracted from the linear fitting procedure for each wavelength.

set of points corresponding to each wavelength was fitted using a linear function and the results of the fitting process are presented in the inset table of Fig. 5. The individual datasets are well described by a linear fit. In the wavelength range 700–1000 nm we observe only a weak wavelength dependence, i.e. datasets are found to feature identical slopes. However, the slope for the 600 ± 5 nm range is found higher by approximately 35 %. The fitted linear curves show positive offsets, which do not surpass 0.022. This very low positive offset value, could potentially be attributed to an intensity drift taking place over the course of almost a full day, which was not observable within the individual time windows, with a duration in the order of few hours, where the optical transmittance was stable. An additional slope, namely 0.83 ± 0.04, which is not included in Fig. 5, was extracted for the wavelength range 625 ± 3 nm, from the present dataset, using the methodology described in Section 3.2, for the purpose of comparison with the literature. The scaling of the optical changes to the number of Cr/V layer repeats, namely N = 23 + 1, in the Cr/V superlattice sample used in the present study yields a normalized slope of 0.034 ± 0.002, for the linear relationship between the scaled optical changes, namely $-\ln\left(\frac{I(c)}{I(c=0)}\right)/N$, and the H/V concentration. This obtained normalized slope value is in excellent agreement with the data presented by Droulias et al. [29], in figure 4 of their corresponding publication, where a normalized slope in the order of 0.19/0.6 = 0.032 can be inferred from the blue line of their plot, for the scaled optical transmittance changes of a deuterated Cr/V superlattice, with a nominal Cr/V ratio of 2/14.

4. Conclusions

In this study the linearity between the hydrogen concentration and the reduction of the optical transmittance, for wavelengths in the region of 600–1000 nm, of Cr/V superlattices, was experimentally confirmed. This result is consistent with previous studies and indicates that optical data can be used to easily extract the hydrogen concentration. For the range 700–1000 nm a weak wavelength dependence was verified, indicating that the extracted slopes can be used as calibration factors between optical transmittance reduction on hydrogenated Cr/V systems

and H/V concentration, in a wide wavelength range. Additionally, the here reported wavelength dependence, for the lower wavelength regime, is attributed to the corresponding wavelength dependence of the changes in the dielectric tensor. Connecting the experimentally observed wavelength dependence to the dielectric tensor and the band structure, through corresponding theoretical calculations or experimental measurements, could be part of future studies. Finally, the present study on the optical properties of the Cr/V system, will allow direct comparison with similar superlattice systems, such as the more extensively studied Fe/V system, in order to assess the proximity effect in epitaxial structures of similar strain states.

Declaration of competing interest

The authors declare that they have no known competing financial interests or personal relationships that could have appeared to influence the work reported in this paper.

Acknowledgments

This work was supported by the Swedish Research Council VR-RFI under contract number #2019–00191.

References

[1] G. Marbán, T. Valdés-Solís, Towards the hydrogen economy? Int. J. Hydrog. Energy 32 (2007) 1625–1637, https://doi.org/10.1016/j.ijhydene.2006.12.017.
[2] L. Schlapbach, A. Züttel, Hydrogen-storage materials for mobile applications, Nature 414 (2001) 353–358, https://doi.org/10.1038/35104634.
[3] A. Züttel, Materials for hydrogen storage, Mater. Today 6 (2003) 24–33, https://doi.org/10.1016/S1369-7021(03)00922-2.
[4] S. Kumar, A. Jain, T. Ichikawa, Y. Kojima, G.K. Dey, Development of vanadium based hydrogen storage material: A review, Renew. Sustain. Energy Rev. 72 (2017) 791–800, https://doi.org/10.1016/j.rser.2017.01.063.
[5] Y. Fukai. Met.-Hydrog. Syst. Basic Bulk Prop., 2nd rev. and updated, ed, Springer, Berlin New York, 2005.
[6] V. Bérubé, G. Radtke, M. Dresselhaus, G. Chen, Size effects on the hydrogen storage properties of nanostructured metal hydrides: A review, Int. J. Energy Res. 31 (2007) 637–663, https://doi.org/10.1002/er.1284.
[7] X. Xin, G.K. Pálsson, M. Wolff, B. Hjörvarsson, Finite-Size Effects: Hydrogen in Fe / V (001) Superlattices, Phys. Rev. Lett. 113 (2014) 046103, https://doi.org/10.1103/PhysRevLett.113.046103.
[8] G. Andersson, B. Hjörvarsson, P. Isberg, Influence of compressive biaxial strain on the hydrogen uptakeof ultrathin single-crystal vanadium layers, Phys. Rev. B 55 (1997) 1774–1781, https://doi.org/10.1103/PhysRevB.55.1774.
[9] G. Reynaldsson, S. Olafsson, H.P. Gislason, Influence of biaxial strain on thermodynamical properties of hydrogen in (001) oriented Mo/V superlattices, J. Alloys Compd. 356–357 (2003) 545–548, https://doi.org/10.1016/S0925-8388(03)00270-6.
[10] E. Veleckis, R.K. Edwards, Thermodynamic properties in the systems vanadium-hydrogen, niobium-hydrogen, and tantalum-hydrogen, J. Phys. Chem. 73 (1969) 683–692, https://doi.org/10.1021/j100723a033.
[11] S. Olsson, B. Hjörvarsson, Effect of biaxial elastic constraints on H − H interactions in ultrathin vanadium, Phys. Rev. B 71 (2005) 035414, https://doi.org/10.1103/PhysRevB.71.035414.
[12] R. Johansson, R. Ahuja, O. Eriksson, B. Hjörvarsson, R.H. Scheicher, Effect of uniaxial strain on the site occupancy of hydrogen in vanadium from density-functional calculations, Sci. Rep. 5 (2015) 10301, https://doi.org/10.1038/srep10301.
[13] G.K. Pálsson, M. Wälde, M. Amft, Y. Wu, M. Ahlberg, M. Wolff, A. Pundt, B. Hjörvarsson, Hydrogen site occupancy and strength of forces in nanosized metal hydrides, Phys. Rev. B 85 (2012) 195407, https://doi.org/10.1103/PhysRevB.85.195407.
[14] G. Alefeld, Ber. Bunsenges., Phase Transitions of Hydrogen in Metals due to Elastic Interaction, Berichte Bunsenges. Für Phys. Chem. 76 (1972) 746–755.
[15] B. Hjörvarsson, G. Andersson, E. Karlsson, Metallic superlattices: quasi two-dimensional playground for hydrogen, J. Alloys Compd. 253–254 (1997) 51–57, https://doi.org/10.1016/S0925-8388(96)02941-6.
[16] P. Isberg, B. Hjörvarsson, R. Wäppling, E.B. Svedberg, L. Hultman, Growth of epitaxial (001) superlattice films, Vacuum 48 (1997) 483–489, https://doi.org/10.1016/S0042-207X(97)00003-1.
[17] S.A. Droulias, G.K. Pálsson, H. Palonen, A. Hasan, K. Leifer, V. Kapaklis, B. Hjörvarsson, M. Wolff, Crystal perfection by strain engineering: The case of Fe/V (001), Thin Solid Films 636 (2017) 608–614, https://doi.org/10.1016/j.tsf.2017.07.005.
[18] J.E. Mattson, E.E. Fullerton, C.H. Sowers, S.D. Bader, Epitaxial growth of body-centered-cubic transition metal films and superlattices onto MgO (111), (011), and (001) substrates, J. Vac. Sci. Technol. Vac. Surf. Films 13 (1995) 276–281, https://doi.org/10.1116/1.579410.
[19] L. Mooij, W. Huang, S.A. Droulias, R. Johansson, O. Hartmann, X. Xin, H. Palonen, R.H. Scheicher, M. Wolff, B. Hjörvarsson, Influence of site occupancy on diffusion of hydrogen in vanadium, Phys. Rev. B 95 (2017) 064310, https://doi.org/10.1103/PhysRevB.95.064310.
[20] T. Burkert, A. Miniotas, B. Hjörvarsson, Hydrogen-induced changes of the local structure in Fe/V (001) superlattices, Phys. Rev. B 63 (2001) 125424, https://doi.org/10.1103/PhysRevB.63.125424.
[21] G.K. Pálsson, A.R. Rennie, B. Hjörvarsson, Examination of the reliability of x-ray techniques for determining hydrogen-induced volume changes, Phys. Rev. B 78 (2008) 104118, https://doi.org/10.1103/PhysRevB.78.104118.
[22] K. Komander, T. Tran, J. Saha, M.V. Moro, G.K. Pálsson, M. Wolff, D. Primetzhofer, Interstitial Hydrogen in Fe / V Superstructures: Lattice Site Location and Thermal Vibration, Phys. Rev. Lett. 127 (2021) 136102, https://doi.org/10.1103/PhysRevLett.127.136102.
[23] K. Komander, M. Moro, J. Saha, M. Wolff, D. Primetzhofer, Hydrogen induced lattice expansion and site occupation analyzed by ion beam methods, Nucl. Instrum. Methods Phys. Res. Sect. B Beam Interact. Mater. at. 486 (2021) 63–67, https://doi.org/10.1016/j.nimb.2020.09.017.
[24] J.N. Huiberts, R. Griessen, J.H. Rector, R.J. Wijngaarden, J.P. Dekker, D.G. De Groot, N.J. Koeman, Yttrium and lanthanum hydride films with switchable optical properties, Nature 380 (1996) 231–234, https://doi.org/10.1038/380231a0.
[25] J. Prinz, G.K. Pálsson, P.T. Korelis, B. Hjörvarsson, Combined light and electron scattering for exploring hydrogen in thin metallic films, Appl. Phys. Lett. 97 (2010) 251910, https://doi.org/10.1063/1.3529465.
[26] R. Gremaud, M. Slaman, H. Schreuders, B. Dam, R. Griessen, An optical method to determine the thermodynamics of hydrogen absorption and desorption in metals, Appl. Phys. Lett. 91 (2007) 231916, https://doi.org/10.1063/1.2821376.
[27] C. Boelsma, L.J. Bannenberg, M.J. Van Setten, N.-J. Steinke, A.A. Van Well, B. Dam, Hafnium—an optical hydrogen sensor spanning six orders in pressure, Nat. Commun. 8 (2017) 15718, https://doi.org/10.1038/ncomms15718.
[28] L.J. Bannenberg, C. Boelsma, H. Schreuders, S. Francke, N.J. Steinke, A.A. Van Well, B. Dam, Optical hydrogen sensing beyond palladium: Hafnium and tantalum as effective sensing materials, Sens. Actuators B Chem. 283 (2019) 538–548, https://doi.org/10.1016/j.snb.2018.12.029.
[29] S.A. Droulias, O. Grånäs, O. Hartmann, K. Komander, B. Hjörvarsson, M. Wolff, G. K. Pálsson, Influence of deuterium-induced volume changes on optical transmission in Fe/V (001) and Cr/V (001) superlattices, Phys. Rev. B 105 (2022) 195438, https://doi.org/10.1103/PhysRevB.105.195438.
[30] K. Komander, M.V. Moro, S.A. Droulias, J. Müggenburg, G.K. Pálsson, T. Nyberg, D. Primetzhofer, M. Wolff, Hydrogen site location in ultrathin vanadium layers by N-15 nuclear reaction analysis, Nucl. Instrum. Methods Phys. Res. Sect. B Beam Interact. Mater. at. 455 (2019) 57–60, https://doi.org/10.1016/j.nimb.2019.05.033.
[31] A.K. Eriksson, A. Liebig, S. Ólafsson, B. Hjörvarsson, Resistivity changes in Cr/V(0 0 1) superlattices during hydrogen absorption, J. Alloys Compd. 446–447 (2007) 526–529, https://doi.org/10.1016/j.jallcom.2007.01.094.
[32] G.K. Pálsson, A.K. Eriksson, M. Amft, X. Xin, A. Liebig, S. Ólafsson, B. Hjörvarsson, Proximity effects on H absorption in ultrathin V layers, Phys. Rev. B 90 (2014) 045420, https://doi.org/10.1103/PhysRevB.90.045420.
[33] Y. Fukai, S. Kazama, K. Tanaka, M. Matsumoto, Hydrogen-induced states in VHx and VDx observed by soft X-ray emission spectroscopy, Solid State Commun. 19 (1976) 507–509, https://doi.org/10.1016/0038-1098(76)90053-3.
[34] L.-C. Duda, P. Isberg, P.H. Andersson, P. Skytt, B. Hjörvarsson, J.-H. Guo, C. Sathe, J. Nordgren, Hydrogen-induced changes of the electronic states in ultrathin single-crystal vanadium layers, Phys. Rev. B 55 (1997) 12914–12917, https://doi.org/10.1103/PhysRevB.55.12914.
[35] G. Andersson, B. Hjörvarsson, H. Zabel, Hydrogen-induced lattice expansion of vanadium in a Fe/V (001) single-crystal superlattice, Phys. Rev. B 55 (1997) 15905–15911, https://doi.org/10.1103/PhysRevB.55.15905.
[36] S.A. Droulias, The effect of nano-confinement on hydrogen uptake in metallic superlattices, Uppsala University, Uppsala, 2018.
[37] P. Haas, F. Tran, P. Blaha, Calculation of the lattice constant of solids with semilocal functionals, Phys. Rev. B 79 (2009) 085104, https://doi.org/10.1103/PhysRevB.79.085104.
[38] Y. Wang, G.K. Pálsson, H. Raanaei, B. Hjörvarsson, The influence of amorphous Al2O3 coating on hydrogen uptake of materials, J. Alloys Compd. 464 (2008) L13–L16, https://doi.org/10.1016/j.jallcom.2007.10.045.
[39] D. Moldarev, K. Komander, R. Holeňák, M. Wolff, D. Primetzhofer, A new setup for optical measurements under controlled environment, Rev. Sci. Instrum. 94 (2023) 035104, https://doi.org/10.1063/5.0142068.
[40] H. Bleichert, H. Wenzl, Die unterschiedliche Löslichkeit der Wasserstoffisotope Protium, Deuterium und Tritium in Vanadium, Phys. Status Solidi B 144 (1987) 361–373, https://doi.org/10.1002/pssb.2221440132.
[41] J.K. Nørskov, Covalent effects in the effective-medium theory of chemical binding: Hydrogen heats of solution in the 3 d metals, Phys. Rev. B 26 (1982) 2875–2885, https://doi.org/10.1103/PhysRevB.26.2875.
[42] F.D. Manchester, A. San-Martin, J.M. Pitre, The H-Pd (hydrogen-palladium) System, J. Phase Equilibria 15 (1994) 62–83, https://doi.org/10.1007/BF02667685.
[43] K.J. Palm, J.B. Murray, T.C. Narayan, J.N. Munday, Dynamic Optical Properties of Metal Hydrides, ACS Photonics 5 (2018) 4677–4686, https://doi.org/10.1021/acsphotonics.8b01243.
[44] P. Ström, D. Primetzhofer, Ion beam tools for nondestructive in-situ and in-operando composition analysis and modification of materials at the Tandem

Laboratory in Uppsala, J. Instrum. 17 (2022) P04011, https://doi.org/10.1088/1748-0221/17/04/P04011.
[45] J.S. Larochelle, A. Désilets-Benoit, G. Borduas, S. Laliberté-Riverin, S. Roorda, M. Brochu, Hydrogen loss during N-15 nuclear reaction analysis of high strength steel, Nucl. Instrum. Methods Phys. Res. Sect. B Beam Interact. Mater. at. 409 (2017) 343–346, https://doi.org/10.1016/j.nimb.2017.03.063.
[46] M. Wilde, K. Fukutani, Hydrogen detection near surfaces and shallow interfaces with resonant nuclear reaction analysis, Surf. Sci. Rep. 69 (2014) 196–295, https://doi.org/10.1016/j.surfrep.2014.08.002.
[47] K. Fukutani, A. Itoh, M. Wilde, M. Matsumoto, Zero-Point Vibration of Hydrogen Adsorbed on Si and Pt Surfaces, Phys. Rev. Lett. 88 (2002) 116101, https://doi.org/10.1103/PhysRevLett.88.116101.
[48] W.A. Lanford, P. Pelicon, B. Zorko, M. Budnar, Use of reference samples for more accurate RBS analyses, Nucl. Instrum. Methods Phys. Res. Sect. B Beam Interact. Mater. at. 190 (2002) 410–413, https://doi.org/10.1016/S0168-583X(02)00464-0.
[49] J.F. Ziegler, M.D. Ziegler, J.P. Biersack, SRIM – The stopping and range of ions in matter (2010), Nucl. Instrum. Methods Phys. Res. Sect. B Beam Interact. Mater. At. 268 (2010) 1818–1823. https://doi.org/10.1016/j.nimb.2010.02.091.
[50] K. Komander, P. Malinovskis, G.K. Pálsson, M. Wolff, D. Primetzhofer, Accurate measurement of hydrogen concentration in transition metal hydrides utilizing electronic excitations by MeV ions, Int. J. Hydrog. Energy 57 (2024) 583–588, https://doi.org/10.1016/j.ijhydene.2024.01.032.